

Methylamines as nitrogen precursors in chemical vapor deposition of gallium nitride

Karl Rönby^{1*}, Sydney C. Buttera², Polla Rouf¹, Seán T. Barry², Lars Ojamäe¹, Henrik Pedersen¹

¹Department of Physics, Chemistry and Biology, Linköping University, SE-581 83 Linköping, Sweden

²Department of Chemistry, Carleton University, 1125 Colonel By Drive, Ottawa, ON, Canada, K1S5B6

*Corresponding author: henrik.pedersen@liu.se; Twitter: @hacp81

Abstract

Chemical vapor deposition (CVD) is one of the most important techniques for depositing thin films of the group 13 nitrides (13-Ns), AlN, GaN, InN and their alloys, for electronic device applications. The standard CVD chemistry for 13-Ns use ammonia as the nitrogen precursor, however, this gives an inefficient CVD chemistry forcing N/13 ratios of 100/1 or more. Here we investigate the hypothesis that replacing the N-H bonds in ammonia with weaker N-C bonds in methylamines will permit better CVD chemistry, allowing lower CVD temperatures and an improved N/13 ratio. Quantum chemical computations shows that while the methylamines have a more reactive gas phase chemistry, ammonia has a more reactive surface chemistry. CVD experiments using methylamines failed to deposit a continuous film, while instead micrometer sized gallium droplets were deposited. This study shows that the nitrogen surface chemistry is most likely more important to consider than the gas phase chemistry when searching for better nitrogen precursors for 13-N CVD.

Introduction

The group 13 nitrides (13-Ns or III-Ns), AlN, GaN, InN and their alloys, form an increasingly important class of semiconductor materials with applications in light emitting diodes (LEDs), laser diodes, high electron mobility transistors (HEMTs), radio frequency (RF) devices, and power transistors. Regardless of the application, one of the most popular methods used to deposit thin layers of 13-Ns is chemical vapor deposition (CVD), where typically trimethyl metal complexes ($M(\text{CH}_3)_3$, where $M = \text{Al, Ga or In}$) and ammonia (NH_3) are used as group 13 and nitrogen precursors, respectively.¹ The reaction pathways of the trimethyl gallium ($\text{Ga}(\text{CH}_3)_3$)/ NH_3 system has been studied earlier, both experimentally and theoretically.^{2,3,4,5,6,7} The studies show a complex gas phase chemistry where both $\text{Ga}(\text{CH}_3)_3$ and NH_3 could decompose to more reactive species that could deposit on the surface or react in the gas phase to form species containing both gallium and nitrogen. $\text{Ga}(\text{CH}_3)_3$ is a Lewis acid due to the empty p-orbital on the metal center and ammonia exists with a free electron pair on the nitrogen, making it a Lewis base; for this reason, Lewis adduct formation of $\text{H}_3\text{N}:\text{Ga}(\text{CH}_3)_3$ is very likely, especially with the Le Chatelier's driving force provided by the large surplus of ammonia in the CVD gas mixture. It has been suggested that such adducts either break up at the high temperatures employed in CVD of 13-Ns or undergo a reaction where a M-N bond is formed with release of methane.^{8,9,10} The formation of $\text{H}_2\text{N}-\text{M}(\text{CH}_3)_2$ could contribute to the growth of GaN by deposition, but might be also detrimental to the CVD process by leading to the formation of parasitic nitride nanoparticles in the gas phase.^{3,9,11,12,13}

Despite the fact that CVD processes for 13-Ns have reached a level of maturity that allows them to be used for industrial production of 13-N based electronics, they typically require a very high NH_3 /13 precursor ratio, typically 100-1000:1 for AlN and GaN¹, and up to 10^5 :1 for InN¹⁴, reflecting poorly tuned CVD chemistry. From a purely thermodynamic point of view, NH_3 will mainly decompose under deposition conditions to highly stable dinitrogen and dihydrogen via the reactive species NH_2 and NH .¹⁵ However, kinetically, NH_2 and NH intermediates only react to form dinitrogen and dihydrogen over longer timescales that are not typically accessible under normal CVD conditions.¹⁶ It has previously been demonstrated that NH_3 has a very low reactivity at typical CVD temperatures for AlN and GaN depositions, and its decomposition by catalysis by iron from the CVD reactor's components has shown to improve ammonia reactivity.¹⁷ The need to use high NH_3 /13 precursor ratios in CVD of group 13 nitrides points to poorly matched precursor kinetics making it interesting to study alternative nitrogen precursors.

This study investigates whether replacing one or more of the N-H bonds (bond dissociation energy: 450 kJ/mol¹⁸) in NH₃ with N-C bonds (bond dissociation energy 356 kJ/mol¹⁹) will lead to a more efficient nitrogen precursor; this change would produce a precursor with weaker bonds and lower symmetry as a result of substituting one or two hydrogens with methyl groups, hopefully increasing its reactivity to deposit group 13 nitride films. Quantum chemical calculations were used to study the possible gas phase chemical reactions in the decomposition of NH_{3-x}(CH₃)_x with x = 0-3. The subsequent surface chemical interactions with the reactive fragments with a GaN surface were also studied using quantum chemical calculations. Since the Lewis adduct formation between acidic group 13 precursors and basic N precursors is an important aspect of the gas phase chemistry for CVD of 13-Ns, it has also been studied by quantum chemical computations in this work. The quantum chemical study is further compared to an experimental CVD study where NH₂CH₃, NH(CH₃)₂ and N(CH₃)₃ were compared to NH₃ as nitrogen precursors in a CVD process with Ga(CH₃)₃.

Methods

Computational details

Quantum chemical calculations were carried out with the Gaussian09 software suite²⁰. The high accuracy Gaussian 4 (G4)²¹ composite method was used for calculations on the gas phase molecular species, which enabled the derivation of thermochemical data for decomposition and adducts reactions. While the G4 method is well established for lighter elements²² there is less experience with its performance for e.g. gallium. Additional calculations using the coupled cluster approach were therefore performed for comparison. The G4 method somewhat overestimates the Ga-CH₃ bond energy (around 10 kJ/mol) compared to those calculated at CCSD(T)/aug-cc-pVTZ²³ level of theory. The calculated adduct formation energies using G4 level of theory, 74.51 kJ/mol for the enthalpy of forming the adduct between NH₃ and Ga(CH₃)₃, are in good agreement with experimental values, -68.20 to -77.82 kJ/mol for the same reaction.^{24,25} The hybrid density functional theory (DFT) B3LYP method with the D3 version of Grimme's empirical dispersion²⁶ and the 6-31G(2df,p) was used as the basis set for the surface interaction studies. For the surface studies, a hydrogen terminated model (0001) surface in the form of a (GaN)₁₃H₃₂ cluster was used (See Fig. S1 in the supporting information). The effect of the size of the cluster on adsorption energies was investigated and are summarized in the supporting information. It was found that the effect was small, i.e. enlarging the cluster changed the adsorption energy by less than 1.84 kJ/mol.

The geometries, for both equilibrium and transition state structures were optimized using the Berny algorithm as implemented in the Gaussian program with standard convergence criteria. The equilibrium structures were confirmed to have zero imaginary vibrational modes by vibrational normal-mode calculations while the transition state structures were confirmed to have one imaginary mode connecting the reactant and product structures. Gibbs free energies were obtained by adding zero-point energies and temperature-dependent energy contributions to the electronic energies along with entropic terms as computed from the vibrational normal-mode frequencies and the optimized geometries.²⁷ An investigation of the error in energies associated with treating the internal rotations as vibrations was performed, see supporting information for details. Due to the small differences in energies (less than 2 kJ/mol for enthalpies and 3.2 kJ/mol for free energies) obtained using the two methods the errors from this approximation were deemed not to significantly affect our conclusions and we chose to not include corrections for the internal rotations in our presented calculations.

Experimental details

The depositions of GaN films were undertaken in a horizontal hot-wall CVD system²⁸ operating at 50 mbar with a carrier gas mixture of palladium membrane purified hydrogen (H₂) and nitrogen (N₂) (99.999%), at a volumetric H₂/N₂ ratio of 6.33. Films were deposited on nominally on-axis 4H-SiC (0001) substrates, cut into 2×2 cm² pieces, washed using standard RCA cleaning solutions²⁹: they were submerged in NH₃:H₂O₂:H₂O 1:1:5, rinsed in deionized water, submerged in HCl:H₂O₂:H₂O 1:1:6, rinsed again in deionized water, and finally dried with dry N₂. Before each CVD experiment, an epitaxial aluminum nitride (AlN) nucleation layer was grown on the SiC substrate using Al(CH₃)₃ (SAFC Hightec EpiPure grade) and NH₃ (99.9999%, further purified using a Nanochem purifier down to < 1 ppb for important contaminants such as water and oxygen) with a flow ratio of NH₃/Al(CH₃)₃ = 1043 at 1200 °C. The temperature was then lowered to 800-1000 °C for the growth of GaN directly on the AlN layer using Ga(CH₃)₃ (SAFC Hightec EpiPure grade) and NH₃, NH₂CH₃ (AGA, 99 %), NH(CH₃)₂ (AGA, 99 %) or N(CH₃)₃ (AGA, 99 %). All methylamines were further purified by a Micro Torr gas filter to reduce water and oxygen to less than 1 ppb.

We note, and would like to point out, that the methylamines, as compared to ammonia, are more challenging to work with in CVD experiments. The lower vapor pressure of the methylamines led, at one point, to condensation of amine in the gas lines and we therefore recommend that the gas lines and mass flow controllers are heated when attempting to replace ammonia with methylamines in a CVD setup.

The morphology of the grown films was characterized using an optical microscope with Nomarski differential interference contrast and by a LEO 1550 Gemini scanning electron microscope (SEM) equipped with a field emission gun using 3-20 kV acceleration. Energy-dispersive X-ray spectroscopy (EDS) was used in the SEM for elemental analysis. An interference method³⁰ was used to determine the thickness of the epitaxial layers. XRD measurements were performed by employing PANalytical EMPYREAN MRD X-Ray diffractometer equipped with a Cu-anode x-ray tube and 5-axis (x-y-z-v-u) sample stage. For the determination of the crystalline structure of the thin films, glancing incidence XRD (GI-XRD) was conducted. For these measurements, capillary optics on the incident beam side and parallel plate collimator on the detector side were used. The Cu K β line was removed by a Ni filter.

Results

Gas phase decomposition of NH_{3-x}(CH₃)_x

The optimized geometries of the NH_{3-x}(CH₃)_x species and their decomposition products are given in Fig. 1. The studied gas phase decomposition reactions are summarized in Scheme 1. In these reaction paths the nitrogen atom consecutively loses a ligand (hydrogen atom or methyl group) and forms more reactive nitrogen radical species. The reactions are labeled “H” and “C” and correspond to the release of a hydrogen (vertical transitions) or a methyl radical (diagonal transitions), respectively. The “RE” reaction is a rearrangement of NCH₃ to methanimine (NHCH₂).

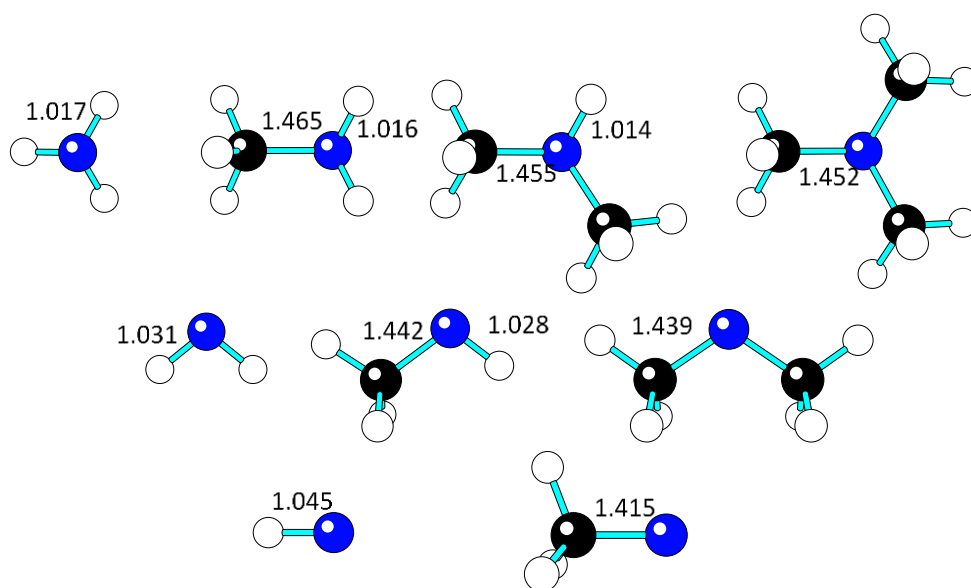
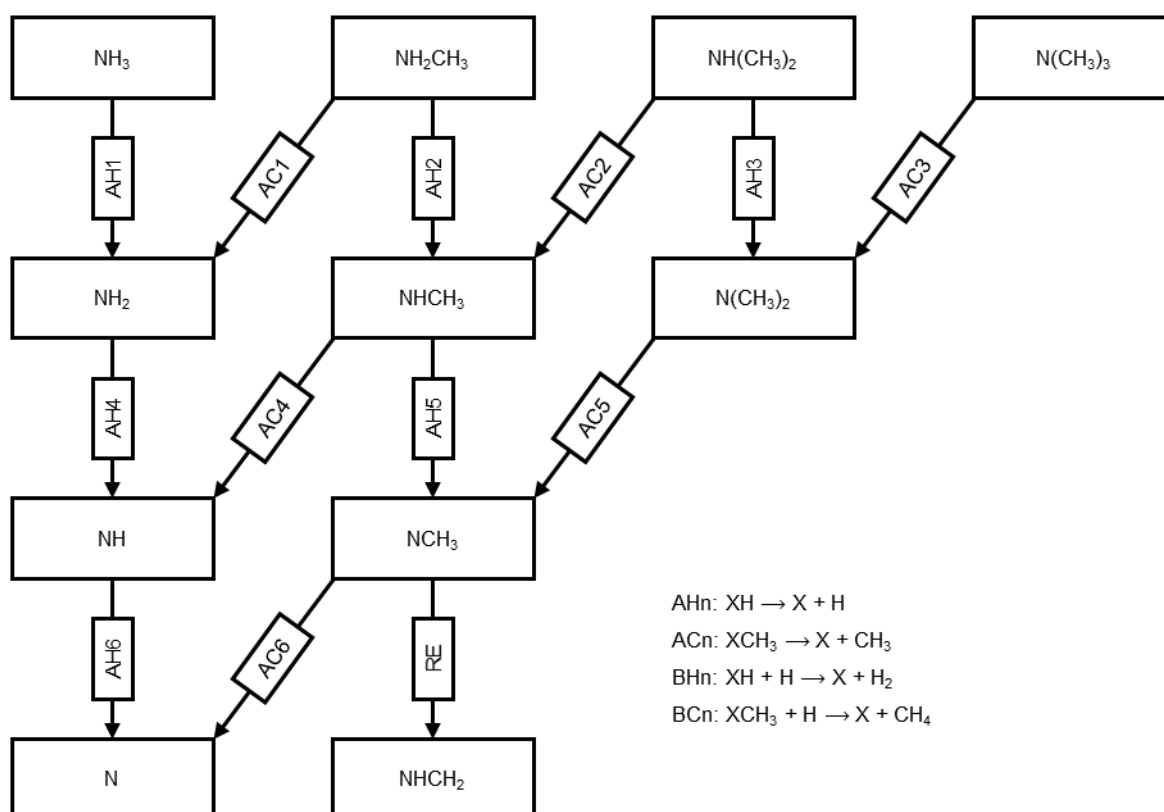


Figure 1: Optimized geometries and bond lengths in Ångström for $\text{NH}_x(\text{CH}_3)_{n-x}$ ($n=3,2,1$) Blue atoms are nitrogen, black are carbon and white are hydrogen.



Scheme 1 – Decomposition pathways for the unimolecular decomposition of methyl amines, $\text{NH}_{3-x}(\text{CH}_3)_x$ with $x = 0-3$. Reactions labeled “AHn” release a hydrogen radical while reactions labeled “ACn” release a methyl radical. Reaction “RE” is a rearrangement.

The energies of the unimolecular decompositions of ammonia and the three methylamines are presented Table 1 and graphically in Figs. S3-S4. All reactions are endoenergetic ($\Delta_r E^{\text{elec}} > 0$) and endothermic ($\Delta_r H^\circ > 0$). All reactions except methyl elimination from $\text{N}(\text{CH}_3)_3$ (AC3) are also endergonic ($\Delta_r G^\circ > 0$), making the reactants more favorable than the decomposition products. The free energies are lower at elevated temperatures due to an increase in entropy, making the difference between $\Delta_r H^\circ$ and $\Delta_r G^\circ$ larger at higher temperatures. In general, the reaction free energy is lower for a loss of methyl than for the loss of a hydrogen radical and the energy difference increases at higher temperatures, which is in line with the bond energies. The triplet spin state of NCH_3 has a lower energy than the singlet state, but the molecule can undergo rearrangement (RE) to the much more stable methanimine (NHCH_2) by migration of a hydrogen from the methyl to the nitrogen, thereby forming a nitrogen-carbon double bond. The structures of these molecules are given in Fig. S5 in the supporting information. The calculated N-C bond length is consistent with the formation of a double bond. This rearrangement was exothermic and had a negative reaction free energy at both STP and CVD conditions at all temperatures. The temperature dependence of the free energy is very small due to the entropy change being small for an internal rearrangement.

Table 1: Reaction enthalpies and free energies for unimolecular decomposition of ammonia and methylamines at CVD conditions; i.e. temperatures in the range 300-1300°C and a total pressure of 50 mbar. All energies are given in kJ/mol. Reaction indices refer to Scheme 1.

React ion index	$\Delta_r H^\circ$						$\Delta_r G^\circ$					
	300°C	500°C	700°C	900°C	1100°C	1300°C	300°C	500°C	700°C	900°C	1100°C	1300°C
AH1	451.2	453.7	455.6	457.1	458.1	458.9	368.7	339.4	309.6	279.5	249.1	218.6
AH2	419.1	421.6	423.5	424.9	426.0	426.7	330.1	298.6	266.5	234.1	201.5	168.7
AH3	395.0	397.6	399.5	400.9	401.9	402.6	299.8	266.2	232.0	197.4	162.6	127.7
AH4	391.8	394.4	396.5	398.3	399.9	401.1	313.9	286.3	258.0	229.4	200.5	171.3
AH5	357.1	358.8	360.1	361.1	361.7	362.1	276.0	247.5	218.5	189.3	159.9	130.5
AH6	338.4	340.8	343.0	345.1	347.0	348.7	269.7	245.3	220.3	194.9	169.2	143.1
AC1	354.5	355.0	354.2	352.6	350.6	348.2	242.9	203.8	164.8	126.1	87.6	49.4
AC2	340.5	340.7	339.7	338.0	335.8	333.3	219.7	177.4	135.3	93.4	51.9	10.7
AC3	329.2	329.2	328.1	326.3	324.1	321.5	199.9	154.7	109.7	65.0	20.6	-23.4
AC4	327.2	327.8	327.2	326.1	324.5	322.6	226.7	191.5	156.3	121.3	86.6	52.0
AC5	302.6	302.0	300.4	298.2	295.7	292.9	195.9	158.7	121.8	85.3	49.2	13.5
AC6	308.5	309.8	310.2	310.1	309.7	309.2	220.4	189.4	158.2	127.0	95.8	64.7
RE	-226.0	-226.6	-227.2	-227.8	-228.3	-228.7	-223.4	-222.4	-221.2	-220.0	-218.6	-217.1

In addition to unimolecular decomposition, there also exists a possibility for ammonia and methylamines to decompose via hydrogen radical assisted abstraction. Hydrogen radicals are abundant under typical CVD conditions given the high temperatures and carrier gas mixture used.³¹ The bimolecular decomposition reactions also follow Scheme 1 with the difference that a hydrogen radical is included as a co-reactant and reacts to form molecular dihydrogen or methane as co-products. The energies of the bimolecular decompositions of ammonia and the three methylamines are given in Table 2 and graphically in Figs. S3-S4. All reactions except the abstraction of a hydrogen from ammonia are exothermic and exergonic ($\Delta_r G^\circ < 0$) at all investigated CVD temperatures. As in the unimolecular case, the effect of increased temperature lowers the reaction enthalpy and free energy. Temperature effects are smaller than

for the unimolecular decomposition due to the smaller change in entropy, since the number of reactants and products are the same. The reaction energy for the removal of a ligand is, as in the unimolecular case, lower for the methyl than the hydrogen.

The mechanism for hydrogen abstraction was assumed to be that initially a hydrogen atom can approach either a hydrogen bonded to the nitrogen or a methyl ligand. As the hydrogen approaches the ligand the bond to the nitrogen is elongated and the ligand can be released in the form of a dihydrogen or methane molecule. Transition states for this mechanism were found, and the corresponding activation energies were computed for the first bimolecular decomposition; the enthalpy and free energy of the transition states relative to the reactants are listed in Table 3 and graphically in Figs. S3-S4. The activation enthalpies for all transition states show very little variance within the temperature range used for CVD, while the activation free energy increases with increased temperature. Noteworthy is that the free energy barrier of hydrogen elimination depends strongly on the number of methyl ligands, while the barrier for the elimination of methane is fairly constant for all the methylamines. The barrier for hydrogen elimination is also lower than the barrier for methane elimination, making the hydrogen elimination the preferred kinetic path, while the reaction free energy makes the methane elimination the preferred thermodynamic path.

Table 2: Reaction enthalpies and free energies for bimolecular decomposition of ammonia and methylamines at CVD conditions of 300-1300°C and 50 mbar. The bimolecular decomposition reactions follow Scheme 1 with the difference that a hydrogen radical is included as a co-reactant and reacts to form molecular hydrogen or methane as a co-product. All energies are given in kJ/mol.

Reaction index	$\Delta_r H^\circ$						$\Delta_r G^\circ$					
	300°C	500°C	700°C	900°C	1100°	1300°	300°C	500°C	700°C	900°C	1100°	1300°
						C						C
BH1	10.4	10.4	9.9	9.0	7.9	6.6	3.6	1.1	-1.2	-3.4	-5.4	-7.3
BH2	-21.7	-21.7	-22.2	-23.1	-24.3	-25.6	-35.0	-39.7	-44.3	-48.8	-53.0	-57.1
BH3	-45.8	-45.7	-46.3	-47.2	-48.4	-49.8	-65.3	-72.1	-78.9	-85.5	-91.9	-98.2
BH4	-49.0	-48.9	-49.2	-49.7	-50.4	-51.2	-51.2	-52.0	-52.8	-53.5	-54.1	-54.5
BH5	-83.7	-84.5	-85.6	-87.0	-88.5	-90.2	-89.1	-90.8	-92.3	-93.6	-94.6	-95.4
BH6	-102.4	-102.5	-102.7	-103.0	-103.3	-103.6	-95.4	-93.0	-90.5	-87.9	-85.4	-82.7
BC1	-88.8	-91.4	-94.4	-97.4	-100.5	-103.4	-101.5	-105.5	-108.8	-111.4	-113.6	-115.3
BC2	-102.8	-105.7	-108.8	-112.0	-115.2	-118.3	-124.7	-131.9	-138.3	-144.1	-149.3	-154.0
BC3	-114.1	-117.2	-120.4	-123.7	-126.9	-130.1	-144.4	-154.6	-163.9	-172.5	-180.5	-188.1
BC4	-116.1	-118.6	-121.3	-124.0	-126.6	-129.0	-117.6	-117.8	-117.2	-116.1	-114.6	-112.7
BC5	-140.7	-144.4	-148.2	-151.8	-155.3	-158.7	-148.5	-150.6	-151.8	-152.2	-151.9	-151.2
BC6	-134.8	-136.6	-138.4	-140.0	-141.3	-142.4	-124.0	-119.9	-115.4	-110.5	-105.4	-100.0

Table 3: Activation enthalpies and free energies for bimolecular decomposition, listed in Table 2, at CVD conditions (300-1300°C and 50 mbar). All energies are given in kJ/mol.

React ion index	$\Delta^{\ddagger}H$						$\Delta^{\ddagger}G$					
	300°C	500°C	700°C	900°C	1100°C	1300°C	300°C	500°C	700°C	900°C	1100°C	1300°C
BH1	52.8	52.2	51.9	51.8	51.7	51.5	124.9	150.2	175.6	201.0	226.4	251.9
BH2	34.6	34.1	34.0	33.9	33.8	33.6	106.5	131.6	156.9	182.2	207.4	232.7
BH3	20.0	19.7	19.6	19.6	19.4	19.3	91.3	116.3	141.3	166.3	191.3	216.3
BC1	132.9	132.3	131.7	131.0	130.2	129.5	204.4	229.4	254.6	280.0	305.4	331.0
BC2	131.7	131.1	130.4	129.7	128.9	128.1	203.2	228.3	253.5	278.8	304.3	329.9
BC3	127.6	127.0	126.3	125.6	124.8	124.0	198.8	223.7	248.8	274.0	299.4	324.9

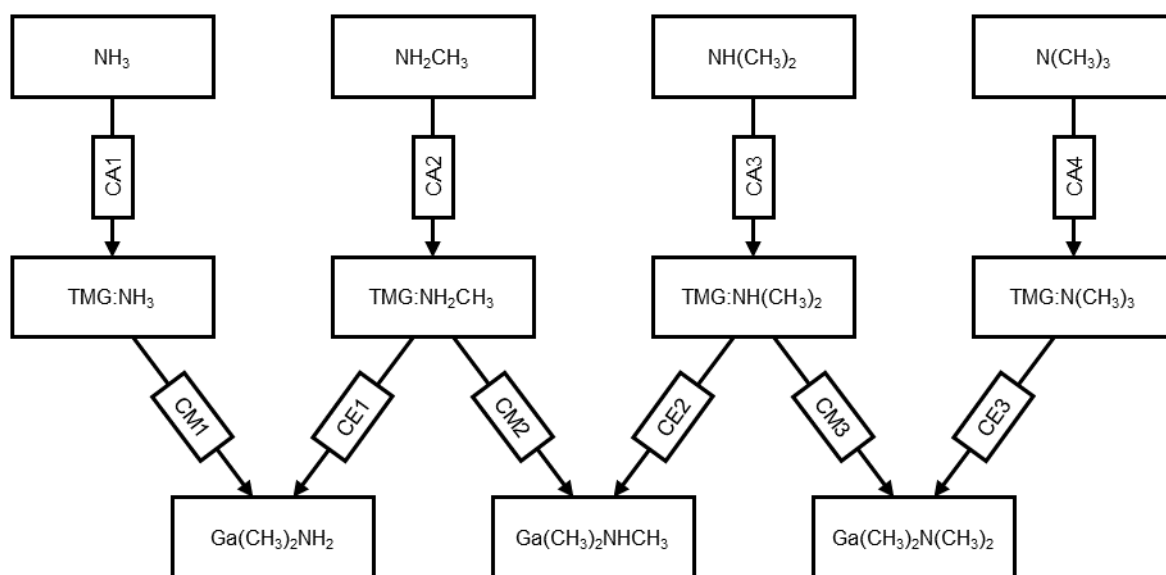
Adduct formation between $NH_{3-x}(CH_3)_x$ and $Ga(CH_3)_3$

The adduct formation between $Ga(CH_3)_3$ and the methylamines with subsequent alkane release reactions are summarized in Scheme 2. The reaction energies are given in Table 4 and graphically in Figs. S3-S4. The adduct formation reactions (CA_n) are all exothermic and exergonic at STP but endergonic for all reactions at CVD temperatures and pressures. The reaction free energy increases as the temperature is increased due to the decrease in entropy from the formed adducts. The reaction free energy for the three first reactions (CA1-3) decreases with increased number of methyl ligands on the nitrogen, possibly due to a stabilizing effect of the positive charge at the nitrogen by the methyl groups. For the last adduct reaction (CA4), the reaction free energy increases, possibly as an effect of steric factors. The optimized geometries for the adducts are given in Fig S6 in the supporting information.

The removal of ligands from the adducts is categorized in two groups: the release of methane (CM_n) and release of ethane (CE_n). At STP and lower CVD temperatures, the removal of both methane and ethane are endothermic and at higher temperatures they are exothermic, except for CE1 which is exothermic at all temperatures. The temperature at which the enthalpy changes sign increases with increasing number of methyl ligands on the nitrogen atom. The reaction free energy is negative for all the removal reactions, and due to the increase in entropy, the reaction is more favorable at higher temperatures. As with the reaction entropy, the reaction free energy is lower for the removal of ethane than for the removal of methane for the mono- and dimethylamine adducts. The sum reaction of adduct formation plus the release of methane or ethane are exothermic at all calculated temperatures; at STP and lower CVD temperatures, the

reaction free energy is negative. Although the release reactions are entropically favorable, the total reaction ($CA_x + CMy/CEy$) has a decrease in entropy. This indicates that the entropy loss in the formation of the adducts is larger than the entropy gain from release of an alkane. This makes the sum reactions less favorable at higher temperatures. The driving force for the adduct formation and release of methane and ethane is the release reactions. The formation of adducts between $NH_{3-x}(CH_3)_x$ and $Al(CH_3)_3$ follows the same trends as the adduct formation with $Ga(CH_3)_3$; all details for adduct formation with $Al(CH_3)_3$ are given in the supporting information.

The alkane release mechanism from the adduct contains a migration of either a hydrogen (methane release) or a methyl (ethane release) from the nitrogen towards one of the methyl groups of $Ga(CH_3)_3$. Simultaneously the nitrogen and gallium atoms are pulled closer to form a covalent bond. The transition state barriers for the alkane release reactions are given in Table 5 and graphically in Figs. S3-S4. The transition state enthalpy is almost constant for all reactions in the CVD temperature range and does also not depend on the number of methyl groups on the nitrogen. The activation enthalpy for the elimination of methane is lower than for the elimination of ethane. The activation free energy barrier of the eliminations has a higher dependence on temperature than the activation enthalpy has, except for reactions CM1 and CE3, and increases slightly with increasing temperatures. The activation free energy of methyl eliminations shows a larger dependence on the number of methyl ligands than the activation free energy of ethane eliminations does. As with the enthalpy barrier, the free energy barrier is higher for the elimination of ethane than for methane, demonstrating that the expected rate of ethane elimination is slower than the rate of methane elimination.



Scheme 2: Reaction pathway diagram of the adduct formation between $\text{NH}_{3-x}(\text{CH}_3)_x$ and $\text{Ga}(\text{CH}_3)_3$ and subsequent alkane elimination reactions. Reactions CA_n are the adduct formation, CM_n are the release of methane, and CE_n are the release of ethane.

Table 4: Reaction enthalpies and free energies for adduct formation between $\text{NH}_{3-x}(\text{CH}_3)_x$ and $\text{Ga}(\text{CH}_3)_3$ and subsequent alkane elimination reactions at CVD conditions: 300°C-1300°C and 50 mbar. All energies are given in kJ/mol. Reaction indices refer to Scheme 2.

Reaction index	$\Delta_r H^\circ$						$\Delta_r G^\circ$					
	300°C	500°C	700°C	900°C	1100°C	1300°C	300°C	500°C	700°C	900°C	1100°C	1300°C
CA1	-73.6	-72.4	-71.0	-69.5	-67.9	-66.4	53.9	98.3	142.3	185.9	229.4	272.6
CA2	-83.0	-80.1	-77.0	-73.9	-70.7	-67.4	36.6	77.9	118.5	158.3	197.7	236.5
CA3	-91.7	-88.7	-85.6	-82.4	-79.2	-76.0	27.4	68.5	108.8	148.4	187.5	226.1
CA4	-95.5	-92.3	-89.2	-86.1	-83.0	-79.8	35.0	80.1	124.3	167.9	211.0	253.5
CM1	1.2	-0.2	-1.7	-3.3	-4.9	-6.6	-98.2	-132.7	-166.8	-200.6	-234.1	-267.4
CM2	7.6	4.4	1.1	-2.2	-5.5	-8.8	-77.0	-106.0	-134.1	-161.6	-188.5	-214.9
CM3	9.8	4.8	-0.2	-5.2	-10.1	-15.0	-60.5	-84.3	-106.7	-128.2	-148.7	-168.6
CE1	-20.5	-23.4	-26.5	-29.7	-33.0	-36.3	-119.7	-153.9	-187.3	-220.1	-252.3	-284.0
CE2	3.4	0.0	-3.4	-6.9	-10.3	-13.6	-91.1	-123.6	-155.2	-186.0	-216.3	-246.1
CE3	13.4	8.0	2.8	-2.4	-7.4	-12.5	-81.1	-113.3	-144.0	-173.7	-202.5	-230.5

Table 5: Activation enthalpies and free energies for alkane elimination from the adducts at CVD conditions: 300-1300°C and 50 mbar. All energies are given in kJ/mol. Reaction indices refer to Scheme 2.

Reaction index	$\Delta^\ddagger H$						$\Delta^\ddagger G$					
	300°C	500°C	700°C	900°C	1100°C	1300°C	300°C	500°C	700°C	900°C	1100°C	1300°C
CM1	144.8	145.8	146.8	147.8	148.7	149.4	145.2	146.2	146.6	146.7	146.5	146.2
CM2	146.2	145.5	144.9	144.2	143.4	142.5	151.4	155.5	158.8	162.4	166.0	169.8
CM3	148.0	147.3	146.6	145.9	145.1	144.2	153.8	158.5	162.2	166.2	170.2	174.5
CE1	386.6	387.1	386.8	386.1	385.0	383.8	389.4	392.8	394.8	396.9	399.0	401.3
CE2	392.4	392.4	391.9	391.1	390.0	388.7	393.7	395.5	396.5	397.6	398.9	400.3
CE3	388.2	388.0	387.3	386.4	385.3	384.0	388.0	388.1	388.1	388.2	388.5	388.9

Surface interactions with GaN (0001)

Adsorption reactions for both $\text{NH}_{3-x}(\text{CH}_3)_x$ and their decomposition products were modeled by allowing the adsorbate to displace a hydrogen at a GaN surface site, releasing a hydrogen radical.



The reaction energies are presented in Table 6 and graphically in Figs. S3-S4; Fig. 2 shows the geometries for the adsorption of the intact $\text{NH}_{3-x}(\text{CH}_3)_x$ species on GaN (0001). In Table 6 the reactions are indexed as Dxy, where x is the total number of ligands attached to the nitrogen and y is the number of methyl ligands. Reaction DRE is the adsorption of the rearranged methanimine. While the adsorptions of NH_3 and NH_2CH_3 are exothermic at the CVD temperatures, undecomposed $\text{NH}(\text{CH}_3)_2$ and $\text{N}(\text{CH}_3)_3$ have a positive reaction enthalpy. The adsorption of all undecomposed species has a positive free energy of adsorption at all CVD temperatures and thus these are not likely to adsorb significantly. The reaction free energy also increases with the temperature for adsorption of all undecomposed species. The computed N – Ga distances and geometries indicate that the adsorption of $\text{N}(\text{CH}_3)_3$ is hindered by steric repulsion due to the methyl groups.

For the first decomposition products, the adsorptions at CVD conditions are exothermic and exergonic, except for $\text{N}(\text{CH}_3)_2$ which is endergonic at high CVD temperature. A lower number of methyl groups on the nitrogen gives a lower adsorption free energy. At higher temperatures, the adsorptions have higher reaction free energies and the effect of temperature is larger as the number of methyl groups is increased. The overall lowest reaction free energy is for the adsorption of NH_2 at all temperatures. For the adsorption of $\text{N}(\text{CH}_3)_2$, the reaction changes from exergonic at lower temperatures to endergonic at temperatures between 900-1100°C. All other reaction free energies are negative indicating favorable reactions.

As with the first decomposition products, all desorptions of second decomposition products are exothermic. The adsorption of NH and NCH_3 are exergonic at lower CVD temperatures and NCH_3 becomes endergonic above 900-1100°C. The reaction free energy is higher for the adsorption of NCH_3 than for NH at all CVD temperatures. The adsorption of the nitrogen radical is both exothermic and exergonic and is less favorable than the adsorption of NH but more favorable than the adsorption of $\text{N}(\text{CH}_3)$, though the free energy approaches that of NH as temperature is increased. The adsorption of NHCH_2 has an adsorption enthalpy close to zero at all CVD conditions and the high adsorption free energy makes adsorption unfavorable.

A radical precursor species is necessary to allow exchange at the hydrogenated GaN surface. The reaction is more thermodynamically likely with a lower number of methyls (i.e., higher number of hydrogen bonded to the precursor nitrogen). In the CVD temperature range, the increase in Δ_rG is more significant for species with a greater number of methyl groups than for ammonia-derived gaseous reactants.

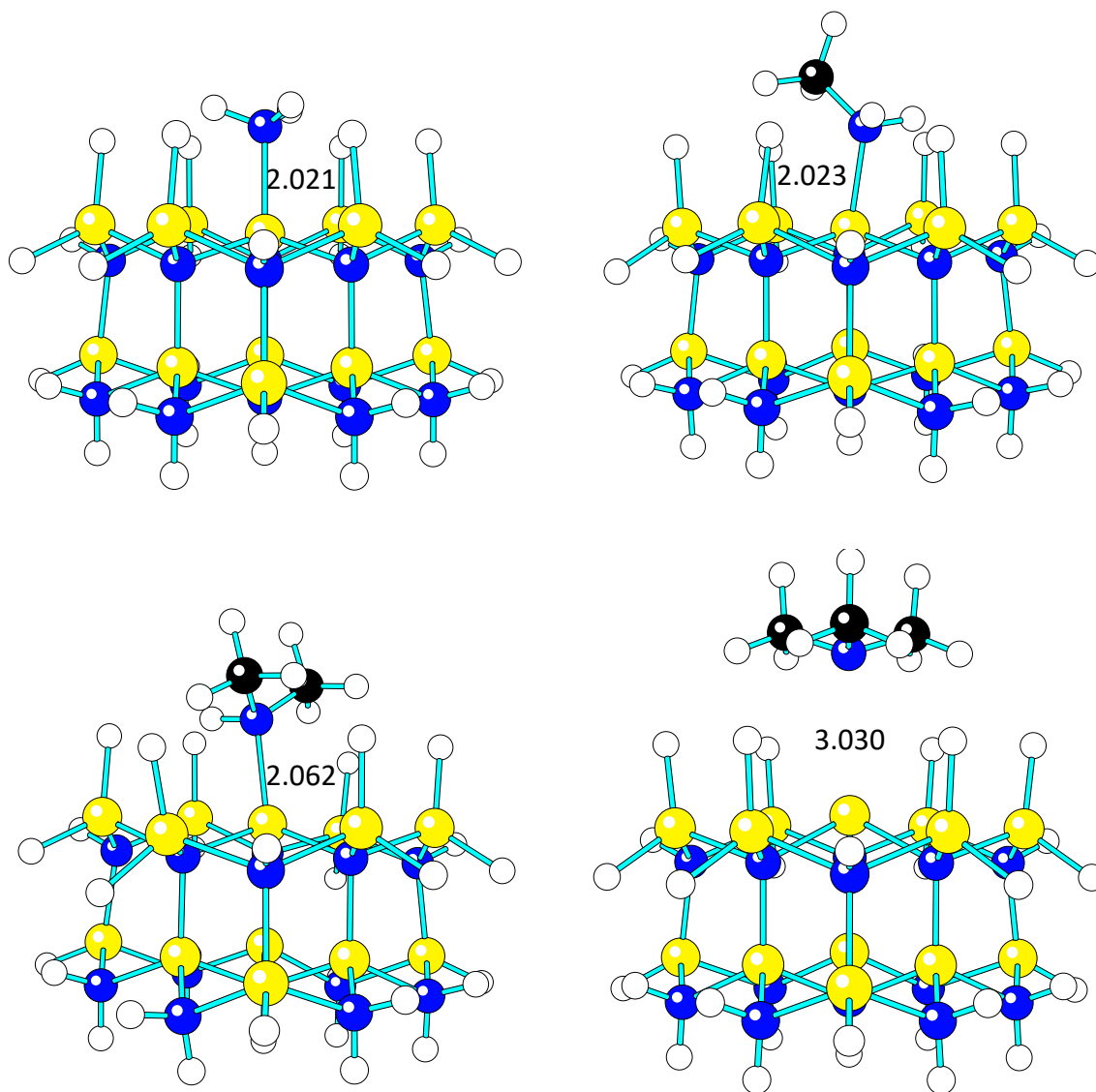


Figure 2: Optimized geometries for the D30 – D33 adsorptions of undecomposed precursors at the GaN (0001) surface. The distance between the Ga at the adsorption site and the N in the precursor is given in Ångströms. Yellow atoms are gallium, blue nitrogen, black carbon and white hydrogen.

Table 6: Reaction enthalpies and free energies for the reaction of ammonia and methylamines with the H-terminated GaN (0001) surface at CVD conditions (300°C-1300°C at 50 mbar). The reactions are indexed as D_{xy}, where x is the total number of ligands attached to the nitrogen and y is the number of methyl ligands. Reaction DRE is the adsorption of the rearranged methanimine. All values are given in kJ/mol.

	$\Delta_r H^\circ$						$\Delta_r G^\circ$					
	300°C	500°C	700°C	900°C	1100°	1300°	300°C	500°C	700°C	900°C	1100°	1300°
	C					C	C					C
D30	-11.6	-9.5	-7.3	-5.2	-3.0	-0.9	38.3	55.3	71.8	87.9	103.6	119.0
D31	-24.0	-23.3	-22.7	-22.2	-21.8	-21.3	49.6	75.2	100.6	125.8	151.0	176.2
D32	4.4	5.1	5.6	6.0	6.3	6.6	87.9	117.0	145.9	174.6	203.4	232.1
D33	79.8	79.6	78.9	77.8	76.6	75.3	144.1	166.6	189.1	211.9	234.8	258.0
D20	-256.8	-254.7	-252.8	-251.0	-249.3	-247.6	-205.6	-188.0	-171.0	-154.3	-138.0	-121.9
D21	-228.6	-226.6	-224.8	-223.1	-221.4	-219.7	-163.2	-140.7	-118.7	-97.1	-75.7	-54.6
D22	-196.5	-196.2	-196.1	-196.0	-196.0	-196.0	-107.3	-76.3	-45.3	-14.3	16.7	47.7
D10	-201.4	-201.7	-202.2	-202.8	-203.5	-204.2	-148.6	-130.2	-111.6	-93.0	-74.2	-55.3
D11	-171.2	-172.1	-173.3	-174.6	-176.1	-177.5	-96.9	-70.9	-44.5	-17.9	8.9	35.9
DRE	-3.7	0.0	3.1	5.7	8.1	10.3	38.3	52.3	65.4	78.0	90.1	101.9
D00	-145.0	-144.8	-145.0	-145.4	-145.9	-146.4	-111.7	-100.1	-88.5	-76.9	-65.2	-53.4

In summary, the computational study shows that the gas phase chemistry for decomposition of $\text{NH}_{3-x}(\text{CH}_3)_x$ becomes more thermodynamically favorable with more methyl groups in the amine precursor. Adduct formation is more favorable with fewer methyl groups in the amine precursor, and the subsequent release of methane or ethane is less favorable as the number of methyl groups is increased. Overall, the gas phase chemistry becomes more favored with higher temperatures. The surface chemistry for adsorption of the $\text{NH}_{3-x}(\text{CH}_3)_x$ becomes more favorable for decomposition products with fewer methyl groups and with lower temperatures. This suggests that $\text{N}(\text{CH}_3)_3$ should be the best nitrogen precursor for gas phase chemistry rendering a higher concentration of more reactive species with less nitrogen species in adducts with gallium species. However, NH_3 is the most favored nitrogen precursor for surface chemistry as

the more methyl groups on the nitrogen atoms, the higher the steric hindrance for chemisorption seems to be.

CVD experiments of GaN using $NH_{3-x}(CH_3)_x$ and $Ga(CH_3)_3$

CVD of GaN was first undertaken with NH_3 and $Ga(CH_3)_3$ to use as a reference. With a N/Ga ratio of 570 and reactor temperatures of 850 °C and 1000 °C, this process resulted in crystalline GaN films with somewhat rough surfaces (Fig. 3). The deposition rate was found to be 44 nm/min at 1000 °C and 37 nm/min at 850 °C.

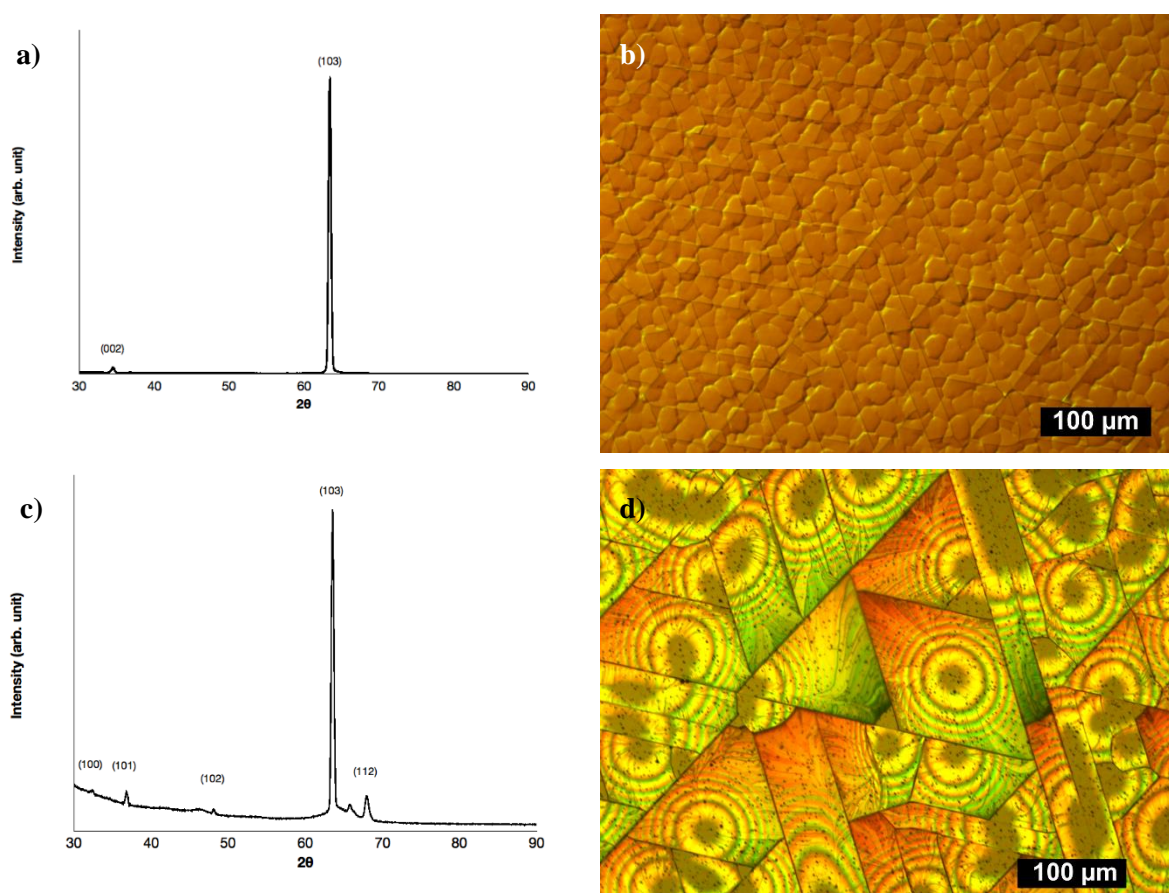


Figure 3: GaN films grown by CVD using $Ga(CH_3)_3$ and NH_3 with N/Ga = 570. Deposition at 1000 °C in panels a) and b) and at 850 °C in panels c) and d) afforded crystalline GaN films, as seen from GIXRD with a rough surface, imaged by optical microscopy.

The same experimental conditions with a reactor temperature of 1000 °C and N/Ga = 570 were then used for CVD experiments with NH_2CH_3 , $NH(CH_3)_2$ and $N(CH_3)_3$. None of these amines yielded any film by SEM or XRD under these conditions. CVD experiments at 850 °C using

NH_2CH_3 and $\text{N}(\text{CH}_3)_3$ with $\text{N}/\text{Ga} = 570$ were performed to probe the possibility of lower CVD temperatures for GaN by $\text{NH}_{3-x}(\text{CH}_3)_x$. These experiments yielded Ga metal droplets (Fig. 4).

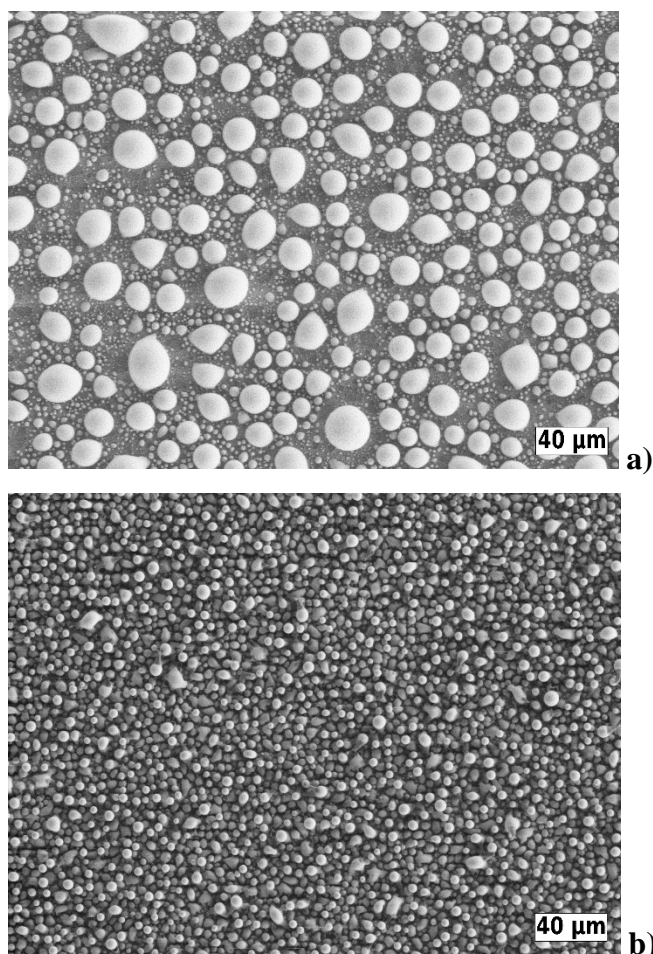


Figure 4: SEM surface micrographs from CVD samples grown at 850 °C using $\text{Ga}(\text{CH}_3)_3$ and a) NH_2CH_3 and b) $\text{N}(\text{CH}_3)_3$ using $\text{N}/\text{Ga} = 570$.

Further attempts to form GaN were undertaken using $\text{N}(\text{CH}_3)_3$ and $\text{Ga}(\text{CH}_3)_3$. The N/Ga ratio was tuned by varying the flow of $\text{N}(\text{CH}_3)_3$ while keeping the flow of $\text{Ga}(\text{CH}_3)_3$ constant at an intermediate deposition temperature of 925 °C. These experiments also resulted in the formation of droplets with the additional growth of cones (Fig. 5). The number of the droplets and cones varied with the N/Ga ratio; a high N/Ga ratio (i.e., higher flow of $\text{N}(\text{CH}_3)_3$) resulted in a lower density of droplets and cones as seen by SEM (Fig. 5). This was also seen by the naked eye as the samples from CVD with a lower N/Ga appeared greyer and more metallic than the samples from CVD with higher N/Ga , which had a shiny appearance on the transparent greenish SiC substrate. The grey coating on the samples could easily be scratched. From EDS (Fig. S8), the droplets were pure gallium, while the cones consisted of gallium with obvious

amounts of nitrogen and carbon. GIXRD of the sample (Fig. S9) show an indication of crystalline gallium in its orthorhombic structure and possible weak XRD peaks from crystalline GaN.

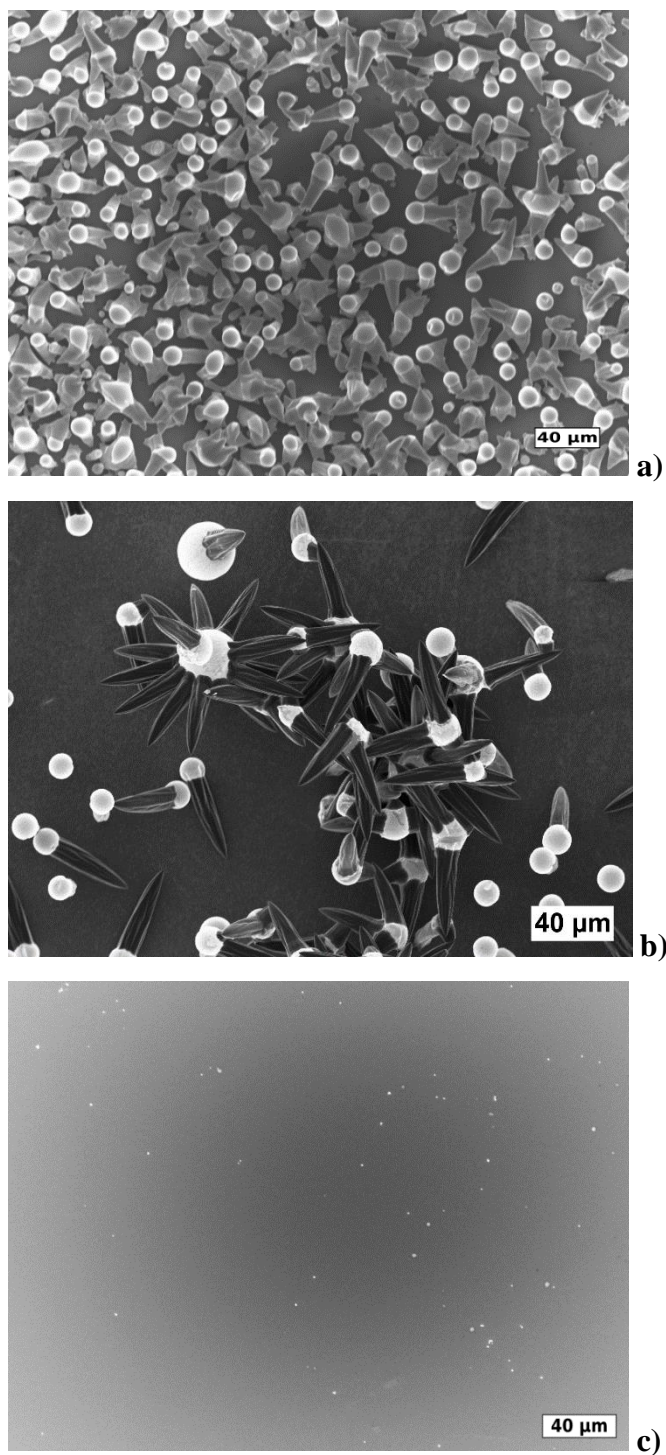


Figure 5: SEM surface micrographs from CVD samples grown at 925 °C from Ga(CH₃)₃ and N(CH₃)₃ using a) N/Ga = 275, b) N/Ga = 570 and c) N/Ga = 1100.

To further study how the concentration of amine affected the deposition, experiments with a N/Ga fixed at 570 and changing the flows, and thereby the partial pressures, of both $\text{N}(\text{CH}_3)_3$ and $\text{Ga}(\text{CH}_3)_3$ were performed (Fig. 6). From these experiments a higher partial pressure of amine, coupled with a higher partial pressure of $\text{Ga}(\text{CH}_3)_3$, rendered larger droplets and fewer cones.

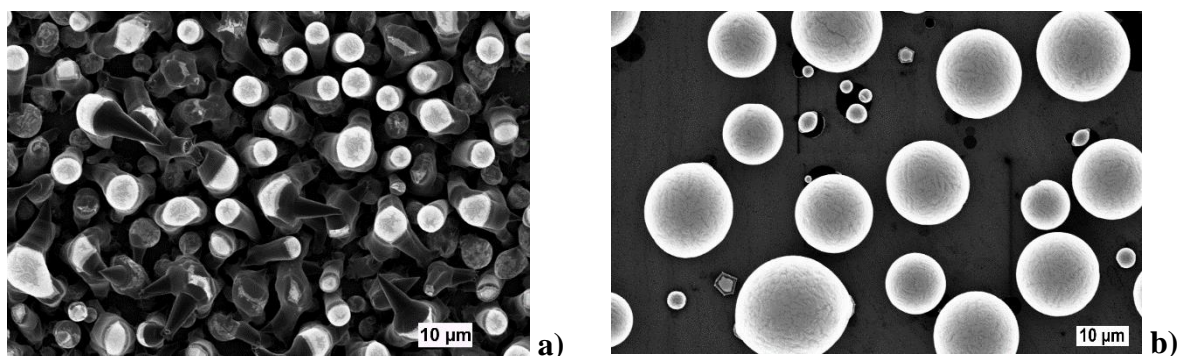


Figure 6: SEM surface micrographs from CVD samples grown at 925 °C using $\text{Ga}(\text{CH}_3)_3$ and $\text{N}(\text{CH}_3)_3$ with N/Ga = 570 and a) low precursor flow ($\text{N}(\text{CH}_3)_3$ at a partial pressure of 2 mbar) and b) high precursor flow ($\text{N}(\text{CH}_3)_3$ at a partial pressure of 8 mbar).

4. Discussion

While the computational study shows that the amines will decompose more easily than ammonia and thereby be more abundant nitrogen precursors in the gas phase at thermodynamic equilibrium for CVD, the experimental study demonstrated that methylamines cannot replace ammonia in CVD of GaN. Rather, methylamines seem to be poor nitrogen precursors as no contiguous GaN films could be grown using them in this study. This is in line with the computational results that showed that methylamines interacted less favorably than amines with the GaN surface (i.e. higher $\Delta_r G$ in Table 6), suggesting that surface chemistry rather than gas phase chemistry is the limiting factor to growing high quality GaN films. Specifically, the exchange of an activated gas phase radical for a surface hydrogen shows less of a thermodynamic driving force as the number of methyl groups increase. This is not due to a difference in the N-H vs. N-Me bond strength (as was originally supposed), but rather due to a difference in radical chemisorption at a surface gallium site. Another factor to consider is that the bimolecular decomposition rates are lower for methylamines than for amines due to higher activation energies (Table 3), which make the methylamine precursor concentrations lower than expected if equilibrium has not been reached in the CVD process. It can also be noted that potentially detrimental adduct derivatives can be formed after both methane and ethane

elimination (Scheme 2) for most of the $\text{Ga}(\text{CH}_3)_3$ -methylamine adducts, but only by methane elimination for the $\text{Ga}(\text{CH}_3)_3$ -ammonia adducts. This could indicate that carbon released as more reactive ethane, rather than less reactive methane, is detrimental to the CVD process of GaN. As our attempts to achieve a continuous GaN film, both by varying N/Ga (through changing the partial pressure of the trimethylamine) and by varying the partial pressures of both trimethylamine and trimethylgallium while keeping a fixed N/Ga, all resulted in formation of droplets and cones. And, a higher partial pressure of the amine, which should be beneficial for adduct formation, always resulted in less growth of cones and formation of larger droplets. Furthermore, EDS mapping of the cones (Fig. S8) shows a significant carbon signal, likely originating from carbon adsorbed on the surface, as the solubility of carbon is very low in both Ga^{32} and GaN^{33} . This can be interpreted as the trimethylamine or its gas phase reaction products, such as ethane, hindering the growth of GaN, leaving droplets of metallic gallium on the surface. This reasoning can be extended to explain why no GaN films were grown using any of the methylamines: the amines or their reaction products could be passivating GaN surfaces, forcing the enhanced formation of metallic gallium droplets.

The presence of metallic droplets appears to favor a VLS-type growth mechanism of cones rather than films. The morphology from SEM, Figs. 5b and EDS mapping Fig. S8, suggests that the metallic gallium droplet is growing while also seeding growth of the cone, causing the growing cone to continually increase in diameter while it grows in length (Fig. 7) This shows similar behavior to the growth of Ga_2O_3 cones using an amidinate precursor and water.³⁴ The material comprising the cone is not fully understood; as no peaks related to gallium oxide could be seen in the GIXRD pattern (Fig. S9) and considering the very weak tendency for gallium to form carbides³⁵ and that nitrogen was detected in the cones by EDS (Fig. S8), a probable material in the cones is an X-ray amorphous gallium nitride. The high amount of carbon detected on the cones in EDS (Fig. S8) could disturb the nitride forming process, leading to an X-ray amorphous gallium nitride structure.

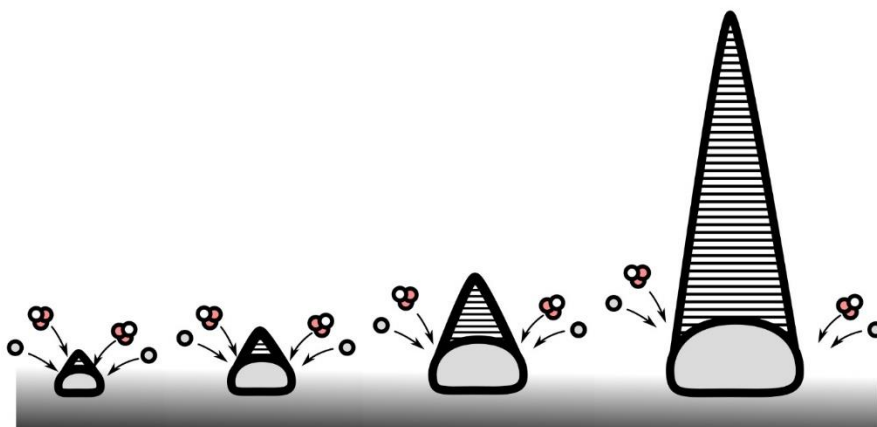
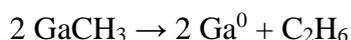


Figure 7: Schematics of a possible growth mechanism for the observed cones.

Although it was observed that low amine flow led to the formation of droplets and cones, and high amine flow led to no deposited species at all, it is unclear what the cause of this is. The formation of gallium metal droplets at the surface occurs more readily at low amine/Ga precursor ratio, $N/Ga = 275$. Perhaps a gallium species, most likely $GaCH_3$ with minor contribution from atomic Ga,³¹ reaches the surface and deposits gallium metal by reductive elimination of ethane:



This would be an irreversible process as there are no oxidizing agents present in the CVD gas mixture. Under low and intermediate amine flow, GaN could then nucleate on the growing droplet surface. Under high amine flow, where there was no apparent GaN formation, the gallium metal could be etched by the overpressure of amine by a subsequent oxidative addition:



Another explanation for the enhanced formation of Ga droplets is a reversible blocking of surface sites by the methylamines reaction products, partially preventing growth of GaN, forcing incoming gallium species to adsorb in a such a way that reductive elimination of alkanes is favored.

Concluding remarks

From quantum chemical computations we find that methylamines show a higher reactivity in the gas phase chemistry of a CVD process for group 13 nitrides than (the currently used precursor) ammonia, while ammonia and its decomposition products show a higher reactivity

towards a GaN surface than methylamines and their decomposition products. CVD experiments where ammonia was replaced by $\text{NH}_{3-x}(\text{CH}_3)_x$ with $x = 1, 2$ or 3 , did not deposit continuous films, and instead the experiments rendered micrometer sized gallium droplets. At some experimental conditions, cone shaped outgrowths from the droplets, probably consisting of X-ray amorphous GaN, were observed. This study shows that in the search to replace ammonia with a more efficient nitrogen precursor in CVD of the group 13 nitrides, allowing for a N/13 ratio closer to unity and lower CVD temperatures, the surface chemistry of the reaction fragments is likely more important than a more reactive gas phase chemistry. The results also suggest that care should be taken to avoid formation of too-reactive hydrocarbon fragments of any new nitrogen precursor.

Acknowledgements

This project was funded by the Swedish foundation for Strategic Research through the project “Time-resolved low temperature CVD for III-nitrides” (SSF-RMA 15-0018). STB and SCB acknowledge the Vinnova VINNMER Marie Curie incoming mobility program for funding for a sabbatical and research visits to Linköping University (Vinnova grant 2015-03714). HP and STB are very grateful for the networking support provided from the COST Action MP1402 ‘Hooking together European research in atomic layer deposition (HERALD) supported by COST (European Cooperation in Science and Technology). LO acknowledges financial support from the Swedish Government Strategic Research Area in Materials Science on Functional Materials at Linköping University (Faculty Grant SFO Mat LiU No. 2009 00971). Supercomputing resources were provided by the Swedish National Infrastructure for Computing (SNIC) and the Swedish National Supercomputer Centre (NSC). Urban Forsberg and Chih-Wei Hsu are gratefully acknowledged for technical assistance with the CVD reactor.

Supporting information

Graphs corresponding to tables 1-6; Ball-and-stick pictures of the optimized molecular geometries; Adduct formation geometries and energies with $\text{Al}(\text{CH}_3)_3$ and $\text{NH}_{3-x}(\text{CH}_3)_x$; EDS and GIXRD measurements of droplets and cones.

References

- (1) Davis, R. F. Organometallic Vapor Phase Epitaxial Growth of Group III Nitrides. *Compr. Semicond. Sci. Technol.* **2011**, *3*, 339-367.
- (2) Mihopoulos T. G.; Gupta V.; Jensen K. F. A reaction-transport model for AlGa₃N MOVPE growth. *J. Cryst. Growth* **1998**, *195*, 733-739.
- (3) Ravasio S.; Momose T.; Fujii K.; Shimogaki Y.; Sugiyama M.; Cavallotti C. Analysis of the gas phase kinetics active during GaN deposition from NH₃ and Ga(CH₃)₃. *J. Phys. Chem. A* **2015**, *119*, 7858-7871.
- (4) Bergmann U.; Reimer V.; Atakan B. An experimental study of the reactions of trimethylgallium with ammonia and water over a wide temperature range. *Phys. Chem. Chem. Phys.* **1999**, *1*, 5593–5599.
- (5) Sekiguchi K.; Shirakawa H.; Chokawa K.; Araidai M.; Kangawa Y.; Kakimoto K.; Shiraishi K. Thermodynamic analysis of trimethylgallium decomposition during GaN metal organic vapor phase epitaxy *Jpn. J. Appl. Phys.* **2018**, *57*, 04FJ03.
- (6) Creighton J. R.; Wang G. T. Kinetics of Metal Organic–Ammonia Adduct Decomposition: Implications for Group-III Nitride MOCVD. *J. Phys. Chem. A* **2005**, *109*, 10554–10562.
- (7) An Q.; Jaramillo-Botero A.; Liu W.-G.; Goddard W. A. Reaction Pathways of GaN (0001) Growth from Trimethylgallium and Ammonia versus Triethylgallium and Hydrazine Using First Principle Calculations *J. Phys. Chem. C* **2015** *119*, 4095–4103.
- (8) Kakanakova-Georgieva, A.; Gueorguiev, G. K.; Stafström, S.; Hultman, L.; Janzén, E. AlGaInN metal-organic-chemical-vapor-deposition gas-phase chemistry in hydrogen and nitrogen diluents: First-principles calculations. *Chem. Phys. Lett.* **2006**, *431*, 346-351.

-
- (9) Nakamura, K.; Makino, O.; Tachibana, A.; Matsumoto, K. Quantum chemical study of parasitic reaction in III–V nitride semiconductor crystal growth. *J. Organomet. Chem.* **2000**, *611*, 514-524.
- (10) Sengupta, D.; Mazumder, S.; Kuykendall, W.; Lowry, S. A. Combined ab initio quantum chemistry and computational fluid dynamics calculations for prediction of gallium nitride growth. *J. Cryst. Growth* **2005**, *279*, 369-382.
- (11) Chen C. H.; Liu H.; Steigerwald D.; Imler W.; Kuo C. P.; Craford M. G.; Ludowise M.; Lester S.; Amano J. A study of parasitic reactions between NH₃ and TMGa or TMAI *J. Electron. Mater.* **1996**, *25*, 1004–1008.
- (12) Moscatelli D.; Caccioppoli P.; Cavallotti C. *Ab initio* study of the gas phase nucleation mechanism of GaN *Appl. Phys. Lett.* **2005**, *86*, 091106
- (13) Hirako A.; Kusakabe K.; Ohkawa K. Modeling of Reaction Pathways of GaN Growth by Metalorganic Vapor-Phase Epitaxy Using TMGa/NH₃/H₂ System: A Computational Fluid Dynamics Simulation Study *Jpn. J. Appl. Phys.* **2005**, *44*, 874–879.
- (14) Ruffenach, S.; Moret, M.; Briot, O.; Gil, B. Recent advances in the MOVPE growth of indium nitride. *Phys. Stat. Sol. A* **2010**, *207*, 9-18.
- (15) Beaumont B.; Gibart P.; Faurie J. P. Nitrogen precursors in metalorganic vapor phase epitaxy of (Al,Ga)N *J. Cryst. Growth* **1995**, *156*, 140–146.
- (16) Konnov A. A.; De Ruyck J. Kinetic Modeling of the Thermal Decomposition of Ammonia. *Combust. Sci. Technol.* **2000**, *152*, 23-37.
- (17) Liu, S. S.; Stevenson, D. A. Growth Kinetics and Catalytic Effects in the Vapor Phase Epitaxy of Gallium Nitride. *J. Electrochem. Soc.* **1978**, *125*, 1161-1169.
- (18) Refers to the N-H bond dissociation energy in the NH₃ molecule. Reference: “Bond dissociation energies in polyatomic molecules,” in CRC Handbook of Chemistry and Physics,

98th Edition (Internet Version 2018), John R. Rumble, ed., CRC Press/Taylor & Francis, Boca Raton, FL.

(19) Refers to the N-C bond dissociation energy in the NH_2CH_3 molecule. Reference: "Bond dissociation energies in polyatomic molecules," in CRC Handbook of Chemistry and Physics, 98th Edition (Internet Version 2018), John R. Rumble, ed., CRC Press/Taylor & Francis, Boca Raton, FL.

(20) Frisch, M. J.; Trucks, G. W.; Schlegel, H. B.; Scuseria, G. E.; Robb, M. A.; Cheeseman, J. R.; Scalmani, G.; Barone, V.; Mennucci, B.; Petersson, G. A.; Nakatsuji, H.; Caricato, M.; Li, X.; Hratchian, H. P.; Izmaylov, A. F.; Bloino, J.; Zheng, G.; Sonnenberg, J. L.; Hada, M.; Ehara, M.; Toyota, K.; Fukuda, R.; Hasegawa, J.; Ishida, M.; Nakajima, T.; Honda, Y.; Kitao, O.; Nakai, H.; Vreven, T.; Montgomery Jr, J. A.; Peralta, J. E.; Ogliaro, F.; Bearpark, M.; Heyd, J. J.; Brothers, E.; Kudin, K. N.; Staroverov, V. N.; Kobayashi, R.; Normand, J.; Raghavachari, K.; Rendell, A.; Burant, J. C.; Iyengar, S. S.; Tomasi, J.; Cossi, M.; Rega, N.; Millam, J. M.; Klene, M.; Knox, J. E.; Cross, J. B.; Bakken, V.; Adamo, C.; Jaramillo, J.; Gomperts, R.; Stratmann, R. E.; Yazyev, O.; Austin, A. J.; Cammi, R.; Pomelli, C.; Ochterski, J. W.; Martin, R. L.; Morokuma, K.; Zakrzewski, V. G.; Voth, G. A.; Salvador, P.; Dannenberg, J. J.; Dapprich, S.; Daniels, A. D.; Farkas, O.; Foresman, J. B.; Ortiz, J. V.; Cioslowski, J.; Fox, D. J. Gaussian 09; Gaussian, Inc.: Wallingford, CT, 2013.

(21) Curtiss, L. A.; Redfern, P. C.; Raghavachari, K. Gaussian-4 theory. *J. Chem. Phys.* **2007**, *126*, 084108.

(22) Curtiss, L. A.; Redfern, P. C.; Raghavachari, K. Assessment of Gaussian-4 theory for energy barriers *Chem. Phys. Lett.* **2010**, *499*, 1–3.

(23) Purvis G. D.; Bartlett R. J. A full coupled-cluster singles and doubles model: The inclusion of disconnected triples *J. Chem. Phys.* **1982**, *76*, 910–1918.

-
- (24) Przhevalskii I. N.; Karpov S. Y.; Markarov Y. N. Thermodynamic properties of group-III nitrides and related species *MRS Internet J. Nitride Semicond. Res.* **1998**, 3, 30
- (25) Creighton J. R.; Wang G. T. Reversible adduct formation of trimethylgallium and trimethylindium with ammonia *J. Phys. Chem. A* **2005**, 109, 133–137.
- (26) Grimme, S.; Antony, J.; Ehrlich, S.; Krieg, H. A consistent and accurate ab initio parameterization of density functional dispersion correction (DFT-D) for the 94 elements H-Pu. *J. Chem. Phys.* **2010**, 132, 154104.
- (27) McQuarrie, D. A.; Simon, J. D. *Molecular Thermodynamics*. University Science Books: Sausalito, CA, **1999**.
- (28) Forsberg, U.; Lundskog, A.; Kakanakova-Georgieva, A.; Ciecchonski, R.; Janzén, E. Improved hot-wall MOCVD growth of highly uniform AlGaIn/GaN/HEMT structures. *J. Cryst. Growth* **2009**, 311, 3007-3010.
- (29) Kern, W.; Puotinen, D. A. Cleaning Solutions Based on Hydrogen Peroxide for use in Silicon Semiconductor Technology. *RCA Review*, **1970**, June, 187-206.
- (30) Kakanakova-Georgieva, A.; Forsberg, U.; Ivanov, I. G.; Janzén, E. Uniform hot-wall MOCVD epitaxial growth of 2 inch AlGaIn/GaN HEMT structures. *J. Cryst. Growth* **2007**, 300, 100-103.
- (31) Danielsson, Ö.; Li, X.; Ojamäe, L.; Janzén, E.; Pedersen, H.; Forsberg, U. A model for carbon incorporation from trimethyl gallium in chemical vapor deposition of gallium nitride. *J. Mater. Chem. C* **2016**, 4, 863-871.
- (32) Fujita, J.; Ueki, R.; Miyazawa, Y.; Ichihashi, T. Graphitization at interface between amorphous carbon and liquid gallium for fabricating large area graphene sheets. *J. Vac. Sci. Technol. B* **2009**, 27, 3063-3066.
- (33) Boguslawski, P.; Briggs, E. L.; Bernholc, J. Amphoteric properties of substitutional carbon impurity in GaN and AlN. *Appl. Phys. Lett.* **1996**, 69, 233-235.

(34) Pallister, P. J.; Buttera, S. C.; Barry, S. T. Self-seeding gallium oxide nanowire growth by pulsed chemical vapor deposition. *Phys. Stat. Sol. A* **2015**, *212*, 1514-1518.

(35) Jansson, U.; Lewin, E. Sputter deposition of transition-metal carbide films - a critical review from a chemical perspective. *Thin Solid Films* **2013**, *536*, 1-24.